Available online at www.sciencedirect.com

SciVerse ScienceDirect

Ceramics International 38 (2012) 2177–2185

CERAMICS INTERNATIONAL

www.elsevier.com/locate/ceramint

The corrosion and microstructure relationship for cement-bonded spinel refractory castables

E.Y. Sako *, M.A.L. Braulio, V.C. Pandolfelli

Federal University of São Carlos, Materials Engineering Department, FIRE Associate Laboratory, São Carlos, SP, 13656-905, Brazil

Received 4 July 2011; received in revised form 19 October 2011; accepted 22 October 2011
Available online 25 October 2011

Abstract

Due to the lack of studies addressing the relationship between chemical and microstructural features and the corrosion resistance of castables containing pre-formed and *in situ* spinel ($MgAl_2O_4$), the main aspects related to the different wear rates of these compositions when in contact with steel ladle slags have not been properly stated. Considering this scenario, this work presents the slag resistance analysis of castables designed by different spinel incorporation routes (*in situ* formation, pre-formed spinel addition and both). A high-iron oxide containing industrial slag was used and the results indicated that the role of the distinct CA_6 ($CaO{\cdot}6Al_2O_3$) distribution in the castable's microstructure before the slag attack was more relevant than the spinel ability as an ion trapper. The location of CA_6 crystals in the *in situ* spinel-forming castable led to a suitable physico-chemical protection of both, the tabular alumina aggregates and the matrix, during the experiment. For the pre-formed spinel-containing castable, the former CA_6 presence only in the matrix resulted in a high dissolution of alumina from the aggregates into the liquid during the corrosion test and a great amount of CA_6 crystals was formed. Cracks were then generated and followed by further cycles of penetration and chemical reactions, which spoiled the refractory's performance.

Keywords: C. Corrosion; D. Spinel castables; E. Refractories

1. Introduction

Adding magnesium aluminate spinel ($MgAl_2O_4$) to refractories for secondary metallurgy has been considered for years as one of the most suitable alternatives to reduce the intensive wear imposed by the steel ladle harsh environment [1–5]. However, many investigations [6–9] have also identified that the spinel incorporation route (*in situ* reaction or pre-formed grains addition) plays a relevant role in some properties, such as thermal-shock resistance, hot modulus of rupture, volumetric stability, and mainly basic slag corrosion resistance.

Chen et al. [8] and Nakamura and colleagues [9] stated that alumina–magnesia (spinel-forming) castables usually present better slag resistance and longer service life in steel ladles when compared to alumina-spinel (spinel-containing) castables. This better performance is related to the mechanism of inhibiting slag penetration, which was suggested by Mori et al. [10]. According to this study, CaO from the CaO–FeO–SiO_2 liquid slag reacts with Al_2O_3 (available in the castable's matrix), giving rise to calcium aluminates compounds (CA_2 and CA_6), whereas FeO_x (and eventually MnO) is incorporated into the spinel structure via solid solutions. The liquid composition then becomes SiO_2-rich and the penetration is lessened due to the increase in its local viscosity. As the *in situ* spinel grains are finer and, thus better distributed throughout the castable microstructure than the pre-formed particles, alumina–magnesia refractories present an efficient behavior when in contact with molten steel ladle slags.

In order to improve the corrosion resistance of alumina-spinel refractory castables, some authors [11,12] investigated the use of pre-formed Al_2O_3-rich spinel. Sarpoolaky and co-authors [11] evaluated the effect of different aggregates on the chemical resistance of low cement castables using an EAF (electric arc furnace) slag and concluded that the addition of 90-wt%-Al_2O_3 spinel grains was beneficial to suppress the molten liquid penetration. Owing to the high amount of Mg^{2+} vacancies, the crystalline structure of those aggregates was

* Corresponding author.
E-mail addresses: eric.ysako@gmail.com (E.Y. Sako), vicpando@ufscar.br (V.C. Pandolfelli).

0272-8842/$36.00
doi:10.1016/j.ceramint.2011.10.061

able to trap a higher content of Fe^{2+} and Mn^{2+} from the slag, reducing the penetration depth. Conversely, Ko [12] found out that the alumina-rich spinel grains actually released the exceeding alumina during firing and were converted to near stoichiometric spinels, and no advantages would, then be associated with this sort of spinel addition.

More recently, Schnabel et al. [13] conducted an extensive comparative evaluation on spinel-forming and spinel containing castables. Confirming previous results in the literature, the material containing *in situ* spinel showed the best performance when considering both penetration depth and wear rate, and the most likely reasons were: the suitable dispersion of *in situ* spinel throughout the microstructure and the spinel volume expansion, which would reduce the open porosity and add a positive effect during the slag attack. Nevertheless, these authors reported that the drawing of conclusions in the direction of better performance of one of the compositions was not straightforward, as they usually presented different formulation concepts.

As described above, most of the investigations carried out in the literature associated the better results of spinel-forming castables with its physical properties. Conversely, few studies have tried to address the chemical aspects such as: (1) the overall microstructural evolution of refractories containing different spinel incorporation routes, and (2) the interactions between this microstructure and the basic slag. Among these few studies, some authors carried out interesting research based on thermochemical calculations using thermodynamic computing simulations [14,15]. The objective of these studies was to predict the full reaction sequence derived from the continuous interaction between the refractory and the molten slag and, then point out the main corrosion mechanisms for spinel-containing and spinel-forming castables.

However, due to various aspects, these investigations did not succeed in solving the question related to the different slag resistance of both compositions. The procedure proposed by Berjonneau et al. [14] considered neither the change in the slag composition due to the partial castable dissolution nor the slag saturation by the refractory's components, which limited the test condition modeling. On the other hand, the improved approach considered by Luz et al. [15] split the thermodynamic modeling in steps and, in each of them, the slag chemical composition changed due to the interaction degree. Following this method, these authors were able to predict and explain satisfactorily some relevant features related to the effect of microsilica and the binder agent on the slag resistance of spinel-forming castable. Nonetheless, as the software considered only the castables overall chemical composition and did not take into account the way in which the oxides were combined, the results attained for the pre-formed spinel-containing castables were exactly the same as for the spinel-forming composition ones.

The most complete analysis of the corrosion resistance of cement-bonded spinel castables was recently published by Braulio et al. [16]. Based on the thermodynamic features stated by Luz et al. [15], the physical property measurements and an overall evaluation of the castable microstructure before the slag attack, a conclusive corrosion mechanism was proposed for the evaluated testing conditions. According to these authors, although the pore diameter distribution seemed to be a key aspect for the penetration resistance, the calcium aluminate phase distribution in the castable matrix and other chemical and microstructural aspects imparted a relevant role in the corrosion behavior.

Hence, the explanation for the distinct slag resistance of alumina–magnesia and alumina-spinel castables might be associated with their different microstructural evolution. The present authors [17] have clearly shown that the calcium hexaluminate (CA_6) crystals distribution in the microstructure of spinel-forming and spinel-containing castables were significantly affected by the previous spinel location. A novel CA_6 formation mechanism was proposed, which included the precipitation of CM_2A_8 ($CaMg_2Al_{16}O_{27}$) as a precursor phase in regions where $MgAl_2O_4$ was dissolved in a CAS liquid. Therefore, the broad distribution of CA_6 observed in the alumina–magnesia castable was most likely related to the previous *in situ* spinel location. On the other hand, for the pre-formed spinel-containing castables, the addition of the magnesium–aluminate was carried out in the matrix, and as a consequence, this was the region where the CA_6 formation took place.

Based on these aspects, this work presents the main features related to the different corrosion behavior of alumina–magnesia and alumina-spinel castables when in contact with steel ladle slags. An in-depth evaluation of the corrosion behavior of four castables containing different spinel incorporation routes (*in situ* formation, pre-formed grains addition and both) was carried out and the different corrosion mechanisms are described, highlighting the importance of understanding the relationship between corrosion and microstructure.

2. Materials and methods

Four high-alumina cement-bonded refractory castables were selected for the corrosion tests. All of them presented the same overall chemical composition, with a total spinel content target of 21 wt%. The raw-materials used to formulate the compositions and their chemical analysis are presented in Table 1.

Table 2 shows the castable compositions containing different *in situ* and pre-formed spinel contents. Aiming to attain a material with 21 wt% of *in situ* (IS) spinel (21 wt% IS composition), 6 wt% of dead-burnt magnesia was added to the matrix in order to react with 7 wt% of reactive alumina and part of the fine tabular alumina ($d < 0.2$ mm) during the heat treatment. On the other hand, 21 wt% of AR78 spinel were used to formulate the castable only containing pre-formed magnesium–aluminate (0 wt% IS). In addition, two intermediate compositions were prepared by simultaneously adding dead-burnt MgO, calcined alumina and synthesized spinel, leading, after firing, to castables with the following rate: 7 wt% *in situ* spinel/14 wt% pre-formed spinel (7 wt % IS); and 14 wt% *in situ* spinel/7 wt% pre-formed spinel (14 wt% IS). The CAC, microsilica and tabular alumina aggregates ($d < 6$ mm) contents were the same for all castables.

Table 1
Chemical composition of the raw materials used to formulate the castables compositions.

Raw materials	Chemical composition (wt%)					
	Al_2O_3	MgO	SiO_2	CaO	Na_2O	Fe_2O_3
Tabular alumina ($d < 6$ mm)[a]	99.5	–	≤0.02	–	0.4	–
Tabular alumina ($d < 0.2$ mm)[a]	99.5	–	≤0.02	–	0.4	–
Calcined alumina CL 370[a]	99.7	–	0.03	0.02	0.1	0.03
Dead-burnt MgO ($d < 45$ μm)[b]	0.35	95.3	1.21	0.44	–	1.8
Synthesized spinel AR78 ($d < 0.5$ mm)[a]	74.0	24.0	0.15	0.24	0.2	0.2
Calcium aluminate cement Secar 71[c]	≥68.5	<0.5	<0.8	≤31.0	<0.5	<0.4
Microsilica 971 U[d]	0.4	0.1	97.5	0.2	0.2	0.1

[a] Almatis, Germany.
[b] Magnesita Refratários, Brazil.
[c] Kerneos, USA.
[d] Elkem, Norway.

Table 2
Composition of the evaluated castables, with different *in situ* (IS) and pre-formed spinel contents.

Raw materials	0 wt% IS	7 wt% IS	14 wt% IS	21 wt% IS
	Content (wt%)			
Tabular alumina ($d < 6$ mm)	62	62	62	62
Tabular alumina ($d < 0.2$ mm)	10	12.7	15.3	18
Calcined alumina CL 370	–	2.3	4.7	7
Dead-burnt MgO ($d < 45$ μm)	–	2	4	6
Synthesized spinel AR78 ($d < 0.5$ mm)	21	14	7	–
Calcium aluminate cement Secar 71	6	6	6	6
Microsilica 971 U	1	1	1	1

The samples' preparation was performed according to the procedure described by Sako et al. [18]. For the corrosion evaluation, the *cup-test* technique was selected and the samples were prepared in a 50 mm × 50 mm cylindrical shape with a 20 mm diameter × 25 mm depth internal hole, as shown in Fig. 1. After pre-firing the samples at 1500 °C for 5 h, their internal holes were filled in with 10 g of a high-iron oxide steel ladle slag in order to perform the tests. The chemical composition of the industrial slag used in this work is presented in Table 3. The sample + slag set was then heated up to 1500 °C and the corrosion experiment was conducted for 2 h in a vertical tube furnace (HTRV100-250/18 GERO, Germany) in air.

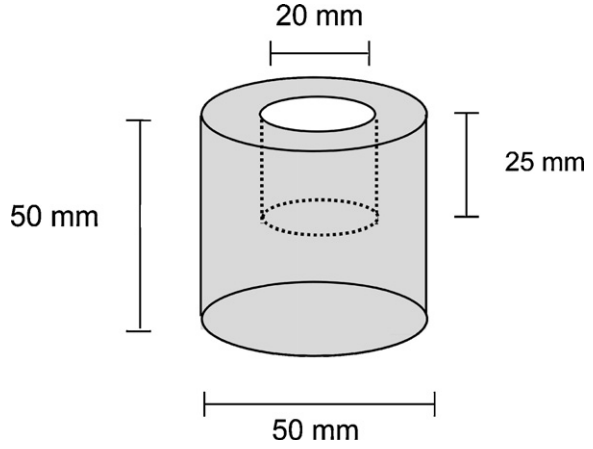

Fig. 1. Illustration of the sample used for the corrosion experiments.

After the experiment, the corroded samples were cut and the cross-sections were used for further microstructural analyses (SEM, JEOL JSM–5900 LV, the Netherlands). In addition, the wear and penetration indexes were calculated in order to measure the corrosion damage using the Image J 1.42q software (Wayne Rasband, National Institutes of Health, USA), according to the procedure described by Braulio et al. [16] and presented in Fig. 2.

The castables' apparent porosity and pore diameter distributions after firing at 1500 °C were also measured using the Archimedes technique in kerosene and the mercury intrusion porosimetry (Aminco, Model 5-7188, USA), respectively.

3. Results and discussions

As described above, four corrosion tests were conducted in order to evaluate the effect of the spinel incorporation route on the castables corrosion resistance. Fig. 3 presents the samples profiles after testing at 1500 °C for 2 h in air for the castables

Table 3
Chemical composition of the industrial steel ladle slag used in this work.

Composition	MgO	Al_2O_3	SiO_2	CaO	MnO	Fe_2O_3
wt%	4.9	1.7	7.5	34.2	3.6	43.6

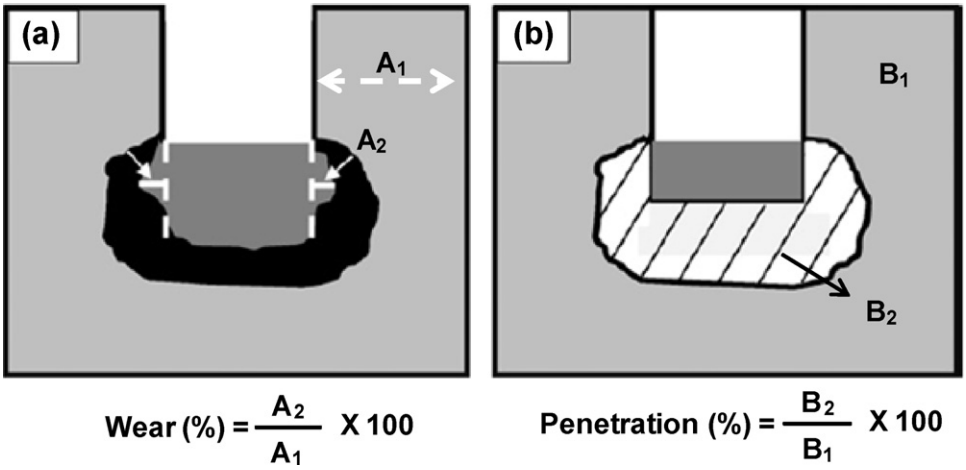

Fig. 2. Description of the wear (a) and penetration (b) indices measurements [16].

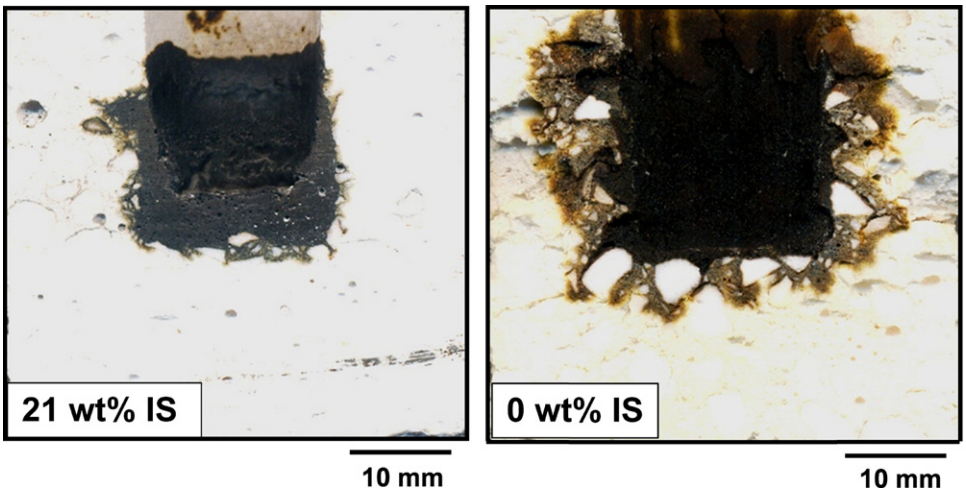

Fig. 3. Cross sections of the samples containing only *in situ* spinel (21 wt% IS) or only pre-formed spinel (0 wt% IS) after the corrosion tests, at 1500 °C for 2 h in air.

containing only *in situ* spinel (21 wt% IS) or only pre-formed spinel (0 wt% IS). The images clearly show the higher corrosion and infiltration resistance of the *in situ* spinel-containing castable in contrast with the poor behavior of the castable in which pre-formed spinel grains were added.

In order to evaluate the results for the four different castables better, Fig. 4 presents the wear and penetration indexes, calculated according to the description in Fig. 2. In this figure, one can observe an increase in the castable corrosion performance as pre-formed spinel grains are gradually replaced by *in situ* ones. The presence of pre-formed spinel grains was responsible not only for an increase in the penetration depth, but also for a higher wear rate.

According to the literature, the main differences regarding the corrosion resistance of spinel-forming and spinel-containing castables could be associated with their different physical characteristics after the heat treatment, such as the open porosity and the average pore size, as they partially define how difficult it is for the slag to infiltrate in the castable's microstructure. Considering this aspect, the open porosity values of the castables fired at 1500 °C for 5 h before the slag attack are presented in Table 4. The open porosity scaled with the *in situ* spinel content in the castables composition, mainly due to the *in situ* spinel formation mechanism. As previously stated in a recent publication by the authors [17], the different

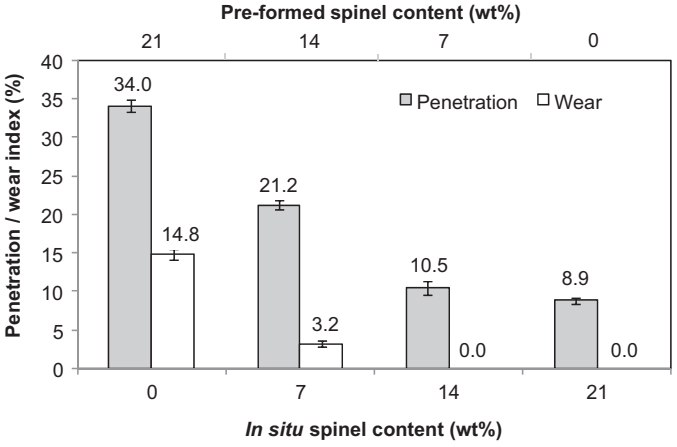

Fig. 4. Slag penetration and wear indexes of the castables containing different *in situ* and pre-formed spinel contents.

Table 4
Apparent porosity of the castables with different *in situ* and pre-formed spinel contents after firing at 1500 °C for 5 h.

	In situ spinel content (wt%)			
	0	7	14	21
Apparent porosity (%)	21.2 ± 0.6	22.5 ± 1.2	23.0 ± 0.4	24.8 ± 0.5

mobility of Al^{3+} and Mg^{2+} ions plays an important role during the $MgAl_2O_4$ generation. As Mg^{2+} diffuses much faster than Al^{3+}, spinel is preferentially formed at the alumina side, whereas pores are left where the MgO grains were previously located. Therefore, the higher the free magnesia content in the castable composition, the higher its open porosity.

Nonetheless, the behavior observed in Table 4 does not match the results presented in Fig. 4, as the corrosion resistance clearly dropped with the pre-formed spinel addition. According to the studies by Zhang and Lee [19], high values of porosity may be related to a high concentration of non-linked and/or small-sized pores, and thus the apparent porosity should not be selected as a good indicative of the slag penetration level. The physical parameter which should be properly correlated to the slag infiltration is then the castable average pore size.

In order to evaluate this aspect, Fig. 5 shows the pore diameter distribution after firing at 1500 °C for the four evaluated castables. Although with a high amount of open pores (Table 4), the microstructures of castables containing *in situ* spinel are characterized by the presence of slightly smaller pores, which matches the improved chemical performance attained with the *in situ* spinel addition. However, when carefully analyzing the castables' average pore sizes (d_{50}), one can notice that all the values are located in a narrow range (less than 2 microns difference), which would not be enough to have a significant impact on the castables' slag resistance. Furthermore, besides the penetration degree, the results in Fig. 4 indicated that the spinel incorporation method affected the slag corrosive wearing as well, suggesting an effect of the castables different microstructural features on the slag–liquid interaction.

Fig. 6 presents the refractories microstructural features before the slag attack. The CA_6 crystals location was directly

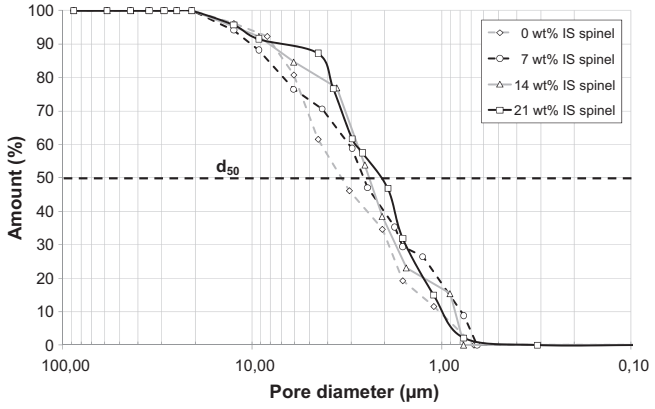

Fig. 5. Pore size distribution for the castables containing different pre-formed and *in situ* spinel contents fired at 1500 °C for 5 h.

related to the previous spinel grains one, due to the complex CA_6 formation mechanism previously reported by the authors [17]. Therefore, for castables containing predominantly pre-formed spinel, which was added to the castable matrix, CA_6 was only found in the matrix. On the other hand, when *in situ* spinel was the major component, CA_6 could be identified both in the matrix and at the border of the tabular alumina aggregates, due to the faster Mg^{2+} mobility which provided spinel formation throughout the castable's microstructure.

Aiming to analyze the effects of these different microstructural aspects on the castables corrosion resistance, SEM images were obtained after the corrosion cup-test experiments (Fig. 7). Based on these microstructures, the significant role of the CA_6 crystals location on the interactions between the liquid slag and the tabular alumina aggregates is pointed out. According to the studies by Mori et al. [10], the corrosion mechanism related to this sort of contact involves initial reactions between Al_2O_3 from the refractory and CaO from the slag (which is present in a high concentration, according to Table 3), leading to the precipitation of calcium aluminate phases. Thus, two mechanisms are proposed in this paper for the aggregate corrosion of the castables containing different methods of spinel incorporation. For the 21 wt% IS castable, the tabular alumina aggregates were mostly coated by a CA_6 layer, as shown in Fig. 6, and thus the alumina remained for the reaction with the slag was reduced, resulting in the formation of a second layer of CA_2. As already reported by Braulio et al. [16], the CA_2 layer was dense and compact, protecting the aggregate from further infiltrations.

Conversely, the tabular alumina aggregates in the pre-formed spinel containing castable (0 wt% IS composition) did not present any previous CA_6 layer. Hence, when the molten slag interacted with those aggregates, a great amount of CA_6 crystals was formed, owing to the high alumina content available. The different reactions involving the corrosion of the Al_2O_3 aggregates for alumina–magnesia and alumina-spinel castables and the values of free energy of formation associated with each of them are described in Eqs. (1) and (2), respectively [15]:

$$CaO \cdot 6Al_2O_{3(s)} + 2CaO_{(l)} \rightarrow 3[CaO \cdot 2Al_2O_3]_{(s)}, \quad \Delta G = -65.1\ \text{kJ/mol} \tag{1}$$

$$6Al_2O_{3(l)} + CaO_{(l)} \rightarrow CaO \cdot 6Al_2O_{3(s)}, \quad \Delta G = -261.1\ \text{kJ/mol} \tag{2}$$

According to the thermodynamics, both reactions (1) and (2) are possible, as their ΔG values are negative, validating, then, the above-proposed corrosion mechanism. It is important to

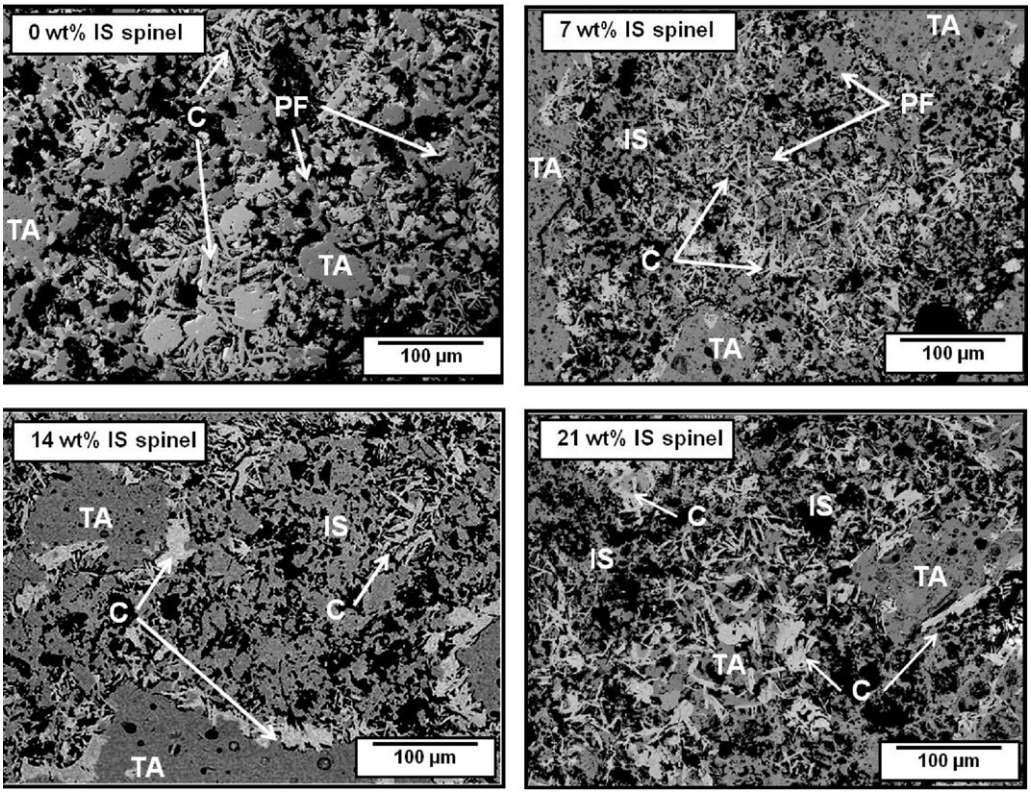

Fig. 6. Microstructure of the castables containing different pre-formed and *in situ* spinel contents fired at 1500 °C for 5 h. TA: tabular alumina, C: CA_6, IS: *in situ* spinel, and PF: pre-formed spinel.

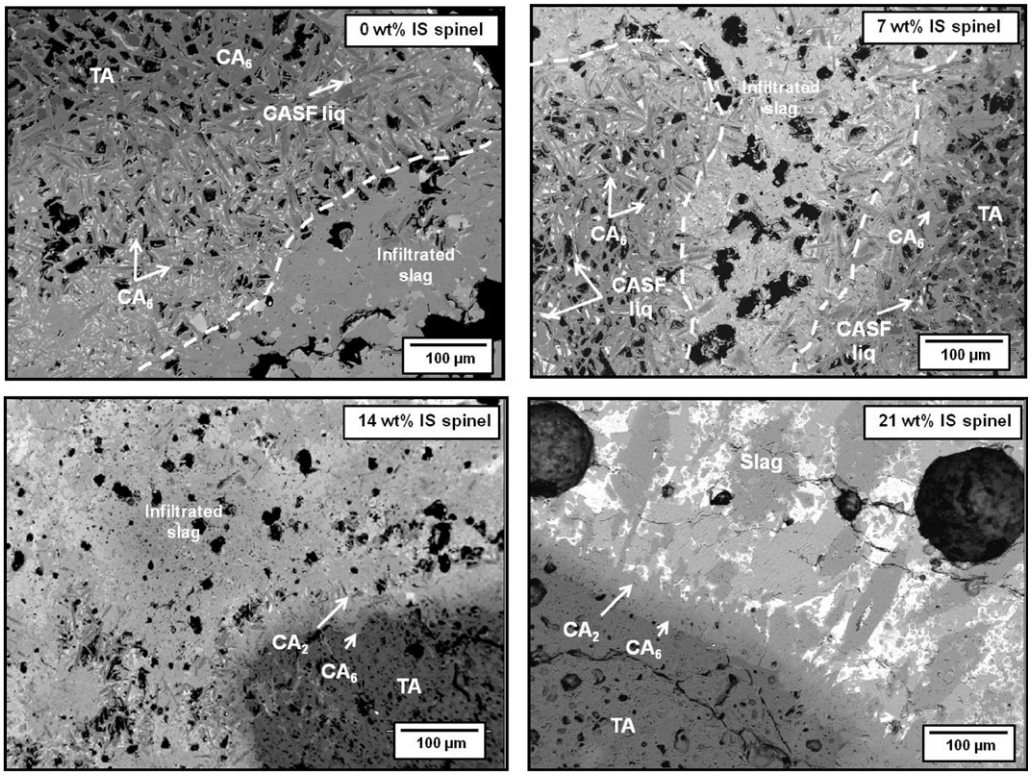

Fig. 7. Microstructure of the corroded samples, highlighting the different interactions between molten slag and tabular alumina (TA) aggregates according to the sort of spinel incorporated. The dashed lines indicate the former borders of the aggregates before the slag attack.

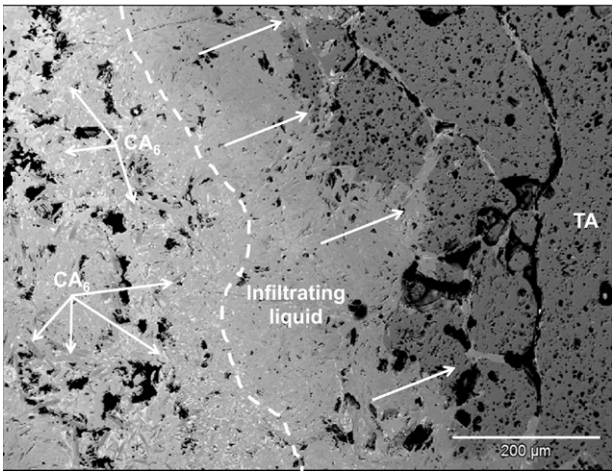

Fig. 8. Corrosion of a tabular alumina aggregate in the alumina-spinel castable (0 wt% IS), highlighting the molten slag infiltration through the cracks generated as a result of excessive CA_6 formation. The dashed line indicates the former boundary of the aggregate.

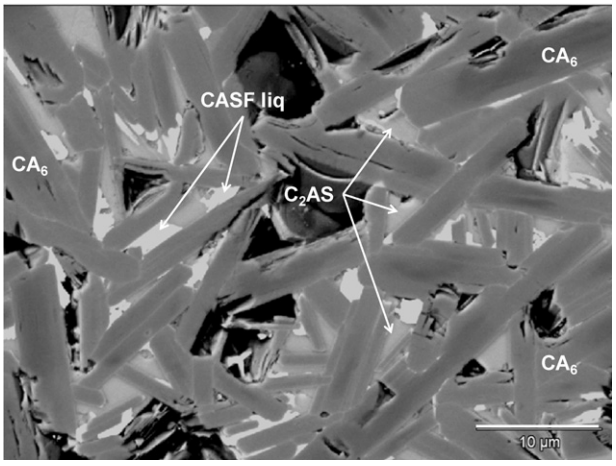

Fig. 9. Detailed image of the area with high concentration of CA_6 in the alumina-spinel (0 wt% IS) corroded sample.

notice that the formation of a CA_2 layer in the 21 wt% IS composition only took place due to the lack of alumina at the border of tabular Al_2O_3 aggregates. In the absence of a pre-reacted area around the aggregates, the dissolution of alumina and the precipitation of CA_6 crystals out of the liquid would be more favorable, as the ΔG value in Eq. (2) is much lower than in Eq. (1). Moreover, the Gibbs free energy values could also be used to explain why CA_6 (and not CA_2) was the product from the interaction between the CaO-rich liquid and the Al_2O_3-rich aggregate in the alumina-spinel castable. When comparing Eq. (2) (precipitation of CA_6) and Eq. (3) (precipitation of CA_2) [15], it is observed that the former presents a lower ΔG value than the latter and, therefore, it is the preferential product observed in the 0 wt% IS micrograph in Fig. 7.

$$2Al_2O_{3(l)} + CaO_{(l)} \rightarrow CaO \cdot 2Al_2O_{3(s)},$$
$$\Delta G = -152.2\,\text{kJ/mol} \quad (3)$$

Regarding the CA_6 phase, its crystals are characterized by the presence of an anisotropic structure [20] and, therefore they usually present a unidirectional grain growth. As a consequence, the CA_6 formation is followed by a significant volumetric expansion ($\Delta V = 3.01\%$) [18,21–23] which led to cracks in the 0 wt% IS aggregates, opening up paths for further cycles of penetration and chemical reactions. For this reason, the tabular alumina aggregates can be found entirely reacted and coated by the CA_6 crystals, as shown in the 0 wt% IS frame in Fig. 7. Thus, although the open porosity of this castable is lower before the slag attack, it drastically increased during the experiment due to the great amount of CA_6 formation, reducing the refractory performance.

The liquid infiltration through the cracks generated in the aggregates is pointed out in Fig. 8, whereas Fig. 9 shows in detail a high CA_6 concentration area in the pre-formed spinel containing castable, highlighting the intergranular presence of gehlenite and glassy phases, which were part of the remaining liquid after the CA_6 precipitation.

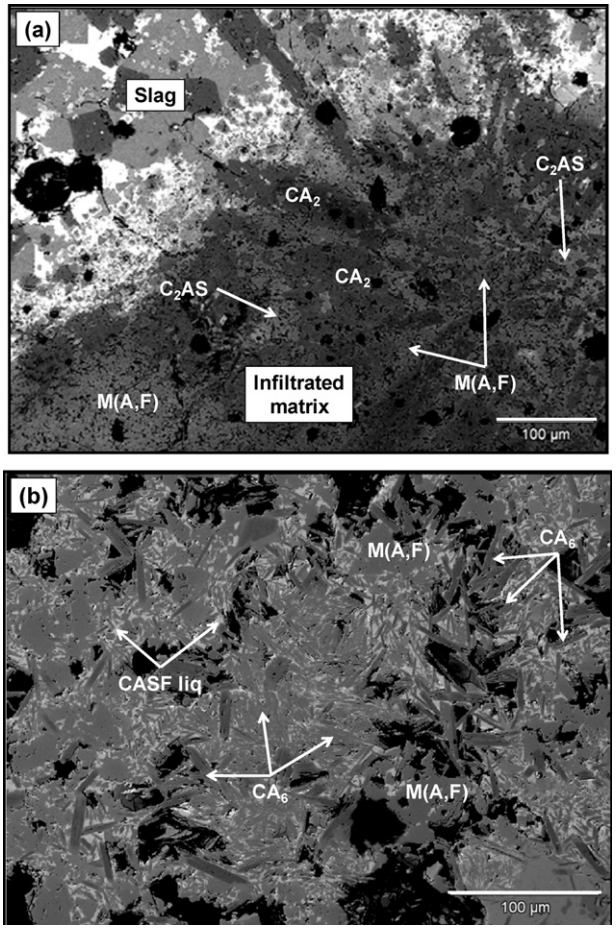

Fig. 10. Infiltrated matrix of (a) alumina–magnesia castable (21 wt% IS) and (b) alumina-spinel castable (0 wt% IS). CA_2 was the major calcium aluminate phase formed in (a), whereas CA_6 was predominant in (b). M(A,F): Magnesium–aluminate spinel with a high amount of iron and manganese oxide in solid solution.

Concerning the castables containing both pre-formed and *in situ* spinel, intermediate situations were identified. Due to their higher *in situ* spinel content, the 14 wt% IS castable behavior was close to the alumina–magnesia one (21 wt% IS).

Conversely, the 7 wt% IS castable features were similar to the alumina-spinel one (0 wt% IS).

Fig. 10 presents the matrix profiles after the molten slag attack for the alumina–magnesia (21 wt% IS) and alumina-spinel castables (0 wt% IS), respectively. Only these two compositions were selected for the matrix evaluation, because the changes in the spinel incorporation method has so far affected proportionally the contact liquid-refractory and, therefore the results for the intermediate compositions could be easily inferred.

The major product from the interaction between molten slag and the refractory matrix was again CA_2 for the alumina–magnesia castable (Fig. 10a). The alumina dissolution from the refractory into the liquid during the corrosion experiment is low for this material, as the aggregates were protected by CA_6 layers before the slag attack and the matrix presented virtually no free alumina (at 1500 °C, the matrix is comprised by *in situ* spinel and CA_6). Hence, CaO from the slag is consumed for the CA_2 precipitation. In addition, magnesium aluminate spinel was also identified in the reacted matrix containing a high amount of iron (25–30 wt%) and manganese (2–3 wt%) ions incorporated in its structure, pointing out the MA spinel's excellent role as an ion trapper. After releasing high contents of calcium and iron oxide to accomplish the reactions above, the slag composition was SiO_2-rich and then crystallized as C_2AS.

In Fig. 10b (0 wt% IS), no CA_2 formation could be found and CA_6 crystals were again the main reaction product, most likely due to the high alumina consumption from the corrosion of aggregates. Additionally, according to a recent publication [24], the Al_2O_3 availability in the 0 wt% IS castable was higher, as no *in situ* spinel formation took place during thermal treatment. Again, the precipitation of an excessive amount of needle-like calcium hexaluminate crystals increased the penetration depth, due to cracks.

A high amount of iron ion was also detected in the spinel structure present in the alumina-spinel reacted matrix, indicating that both pre-formed and *in situ* spinel were likewise efficient in trapping deleterious ions from the molten slag. Therefore, the corrosion behavior of cement-bonded castables containing different sorts of spinel incorporation was exclusively related to their different microstructural development, even though the initial chemical compositions were the same.

4. Conclusions

The results attained indicated the main aspects for the better corrosion and slag penetration resistance by the replacement of pre-formed spinel by *in situ* spinel in cement-bonded high-alumina castables. The higher amount of smaller pores had virtually no meaningful effects on the performance of *in situ* spinel-forming castables, which was more sensitive to chemical aspects. For *in situ* spinel castables, the location of CA_6 crystals through the microstructure before the slag attack resulted in a suitable protection of tabular alumina aggregates during the experiment, inhibiting the more favorable CA_6 precipitation as the interaction product. Consequently, a second dense and compact CA_2 layer was formed both at the aggregates and in the matrix, suppressing further infiltrations.

On the other hand, as CA_6 was only found in the matrix of the pre-formed spinel-containing castable, the alumina coarse aggregates were easily dissolved in the molten slag, resulting in the precipitation of a large amount of needle-like CA_6 crystals. Owing to its volumetric expansion, the CA_6 formation generated cracks, which opened up paths for further cycles of penetration and chemical reactions.

The castables containing both pre-formed and *in situ* spinel presented intermediate behaviors, which were in tune with the major sort of spinel present in the composition. The microstructural features of the 14 wt% IS castable was close to the alumina–magnesia one, whereas the results for the 7 wt% IS were very similar to the alumina-spinel ones.

Thus, although the castables presented the same overall chemical composition and the same potential efficiency in trapping ions from the slag, regardless of the source of selected spinel, the corrosion resistance was considerably different. The results attested the importance of the correct understanding of the castables microstructural evolution in order to predict the slag–refractory interaction products and avoid undesired failures due to corrosive wearing.

Acknowledgements

The authors are grateful to the Federation for International Refractory Research and Education (FIRE) and the Brazilian Research Funding CNPq for supporting this work. The discussions with Dr. E. Zinngrebe and Dr. S. R. van der Laan, both from Tata Steel Europe, Ijmuiden, The Netherlands, were also deeply appreciated.

References

[1] B. Nagai, O. Matsumoto, T. Isobe, Development of high-alumina castable for steel ladles (findings on spinel formation in alumina–magnesia castables), Taikabutsu Overseas 10 (1) (1998) 23–28.
[2] M. Tawara, K. Fujii, T. Taniguchi, M. Hagiwara, T. Kibayashi, M. Tanaka, Application of alumina–magnesia castable in high-temperature steel ladles, Taikabutsu 45 (6) (1995) 291–294.
[3] M. Kobayashi, K. Kataoka, Y. Sakamoto, I. Kifune, Use of alumina–magnesia castables in steel ladle sidewalls, Taikabutsu Overseas 17 (3) (1997) 39–44.
[4] S. Itose, M. Nakashima, T. Isobe, I. Shimizu, Improvement in the durability of alumina-spinel steel ladle castable containing spinel fine powder, Journal of the Technical Association of Refractories – Japan 22 (1) (2002) 26–30.
[5] D. Schmidtmeier, G. Büchel, A. Buhr, Magnesium aluminate spinel raw materials for high performance refractories for steel ladles, Materialy Ceramiczne 61 (4) (2009) 223–227.
[6] S. Mukhopadhyay, P.K. Das Poddar, Effect of pre-formed and in situ spinels on microstructure and properties of a low cement refractory castable, Ceramics International 30 (2004) 369–380.
[7] Y.-C. Ko, Properties and production of Al_2O_3-spinel and Al_2O_3–MgO castables for steel ladles, CN-Refractories 6 (1) (2002) 51–56.
[8] S.-K. Chen, M.-Y. Cheng, S.-J. Lin, Y.-C. Ko, Thermal characteristics of Al_2O_3–MgO and Al_2O_3-spinel castables for steel ladles, Ceramics International 28 (2002) 811–817.

[9] R. Nakamura, T. Kaneshige, K. Matsumura, H. Sasaki, 1999. The current status of ladle castables and application of clean shot system to steel ladles. Shinagawa Technical Report No. 42, 7–14.
[10] J. Mori, N. Watanabe, M. Yoshimura, Y. Oguchi, T. Kwakami, Material design of monolithic refractories for steel ladle, American Ceramic Society Bulletin 69 (7) (1990) 1172–1176.
[11] H. Sarpoolaky, S. Zhang, W.E. Lee, Corrosion of high alumina and near stoichiometric spinels in iron-containing silicate slags, Journal of the European Ceramic Society 23 (2003) 293–300.
[12] Y.-C. Ko, Influence of the characteristics of spinels on the slag resistance of Al_2O_3–MgO and Al_2O_3-spinel castables, Journal of American Ceramic Society 83 (9) (2000) 2333–2335.
[13] M. Schnabel, A. Buhr, R. Exenberger, C. Rampitsch, Spinel: in situ versus preformed – clearing the myth, Refractories World Forum 2 (2) (2010) 87–93.
[14] J. Berjonneau, P. Pringent, J. Poirier, The development of a thermodynamic model for Al_2O_3–MgO refractory castable corrosion by secondary metallurgy steel ladle slags, Ceramics International 35 (2) (2009) 623–635.
[15] A.P. Luz, A.G. Tomba Martinez, M.A.L. Braulio, V.C. Pandolfelli, Thermodynamic evaluation of spinel containing refractory castables corrosion by secondary metallurgy slag, Ceramics International 37 (2011) 1191–1201.
[16] M.A.L. Braulio, A.P. Luz, A.G. Tomba Martinez, C. Liebske, V.C. Pandolfelli, Basic slag attack of spinel-containing refractory castables, Ceramics International (2011), doi:10.1016/j.ceramint.2011.02.007.
[17] E.Y. Sako, M.A.L. Braulio, E. Zinngrebe, S.R. vdLaan, V.C. Pandolfelli, In-depth microstructural evolution analyses of cement-bonded $MgAl_2O_4$-containing castables – novel insights regarding to the spinel and CA_6 formation, Journal of American Ceramic Society (2011), submitted for publication.
[18] E.Y. Sako, M.A.L. Braulio, D.H. Milanez, P.O. Brant, V.C. Pandolfelli, Microsilica role in the CA_6 formation in cement-bonded spinel refractory castables, Journal of Materials Processing Technology 209 (2009) 5552–5557.
[19] W.R. Lee, S. Zhang, Melt corrosion of oxides and oxide–carbon refractories, International Materials Reviews 44 (3) (1999) 77–104.
[20] M.K. Cinibulk, Hexaluminates as a cleavable fiber–matrix interphase: synthesis, texture development, and phase compatibility, Journal of European Ceramic Society 20 (2000) 569–582.
[21] M.A.L Braulio, D.H. Milanez, E.Y. Sako, L.R.M. Bittencourt, V.C. Pandolfelli, Expansion behavior of cement bonded alumina–magnesia refractory castables, American Ceramic Society Bulletin 86 (12) (2007) 9201–9206.
[22] J.M. Auvray, C. Gault, M. Huger, Evolution of elastic properties and microstructural changes versus temperature in bonding phases of alumina and alumina–magnesia refractory castables, Journal of European Ceramic Society 27 (2007) 3489–3496.
[23] M.A.L. Braulio, L.R.M. Bitttencourt, V.C. Pandolfelli, Engineered expansion routes for alumina–magnesia castables, Ceramic Forum International 85 (2008) E77–E82.
[24] E.Y. Sako, M.A.L. Braulio, P.O. Brant, V.C. Pandolfelli, The impact of pre-formed and in situ spinel formation on the physical properties of cement-bonded high-alumina refractory castables, Ceramics International 36 (2010) 2079–2085.